machines

MDPI

Article

Simulation Study on Arc Temperature of Urban Rail DC Pantograph-Catenary and Arc Ablation of Contact Line

Xiaoying Yu, Ze Wang *, Mengjie Song, Liying Song, Junrui Yang and Yang Su

School of Automation & Electrical Engineering, Lanzhou Jiaotong University, Lanzhou 730070, China
* Correspondence: wz12222024@163.com

Abstract: The high temperature generated by the DC pantograph-catenary arc of urban rail systems will aggravate the wear of the pantograph-catenary system. When the ablation intensifies, it will lead to disconnection accidents on the contact line. In this paper, through the establishment of a pantograph-catenary arc model and contact line arc ablation model, considering the flow of the molten pool, it is reported that the temperature distribution of the pantograph-catenary arc is axisymmetric. With the increase in the arcing time, the maximum temperature of the arc increases. The heat flux density of the arc injection contact line presents a Gaussian distribution and is positively correlated with the arcing time. The high-temperature area of the contact line and the distribution of the molten pool show an approximate arc shape. The velocity of the molten pool shows a symmetrical distribution about the center of the electrode. The area, depth, and radius of the molten pool of the contact line increase with an increase in the arcing time, and the radius of the molten pool is always greater than the depth of the molten pool. The work presented in this paper is helpful to further our understanding of the basic physical process of pantograph-catenary arc ablation of contact lines.

Keywords: urban rail transit; pantograph-catenary arcing; temperature distribution; contact line; molten pool

Citation: Yu, X.; Wang, Z.; Song, M.; Song, L.; Yang, J.; Su, Y. Simulation Study on Arc Temperature of Urban Rail DC Pantograph-Catenary and Arc Ablation of Contact Line. *Machines* **2024**, *12*, 514. https://doi.org/10.3390/machines12080514

Academic Editors: Parviz Famouri and Ahmed Abu-Siada

Received: 19 June 2024
Revised: 17 July 2024
Accepted: 26 July 2024
Published: 29 July 2024

1. Introduction

Urban rail transit has a strong carrying capacity, making it a convenient and environmentally friendly mode of transportation. Urban rail transit has high transportation efficiency and conforms to the current mainstream green environmental protection development concepts around the world. It can be seen that such a system is very suitable for use in many large and medium-sized cities in the world; thus, urban rail transit plays a vital role in promoting urban development, and its safe and efficient operation is directly related to the travel, work, and life of urban residents [1,2].

The power provided by the pantograph-catenary system is essential for the normal operation of these trains [3]. However, in the actual operation of the train, the arcing of the pantograph-catenary system is inevitable due to the operation of raising and lowering the pantograph, the vibration in the vehicle body, and the unevenness of the track. The arc will be accompanied by a sharp increase in temperature at the moment of arcing. The heat generated will even exceed the melting point of the contact line material, causing severe ablation on the surface of the contact line, which eventually accelerates its aging and retirement from service [4–6]. In addition, the DC pantograph-catenary arc has a long duration, a high arcing rate, and stable combustion, which will aggravate the high-temperature impact of the arc [7]. During the daily operation of the pantograph-catenary system, although the contact line wears less than the pantograph slide plate, the maintenance period for the contact line is longer, which also brings its own safety risks to train operation. A simulation study on the arc temperature of urban rail DC pantograph-catenary and arc ablation of the contact line can be used to construct a whole picture of the pantograph-catenary arc and analyze the internal formation mechanism in the ablation process of electrical contact materials [8].

Therefore, studying the content of this article will be of great significance in the future to suppress pantograph-catenary arcing, evaluate the service life of pantograph-catenary system materials, and improve arc ablation resistance.

At present, a large number of scholars have carried out relevant research work on the arc, the arc ablation of electrode contact materials, and the phase transition of materials. Toktaliev et al. conducted parameter experiments and numerical studies on the arc motion process of adding a transverse constant magnetic field in static air. The numerical study used a two-dimensional numerical simulation method under an MHD approximation to explore the temperature and flow characteristics of the arc [9]. However, this study did not calculate the electrode temperature rise and the formation of the molten pool under the action of the arc. Sunar Ö et al. experimentally studied the effect of arc discharge on the surface ablation of contact line materials. By comparing the samples without arc damage, it was found that arc damage was the main factor that greatly reduced the fatigue life of the contact line [10]. However, this study failed to examine the internal formation mechanism of the arc ablation of the contact line. Based on the coupled ablation model of the pantograph-catenary arc and pantograph-catenary material, Wu Yuxin analyzed the temperature distribution of the contact line and the change rule of a molten pool under different arc currents and different arc gaps [11], but these studies did not consider the flow of the molten pool in a contact line. In terms of the phase change analysis of PCM materials, Sabine Moench et al. established an enhanced model considering the flow of the molten pool based on the enthalpy-porosity method and compared it with the default model in COMSOL Multiphysics. It was found that ignoring the flow of the molten pool would lead to inaccurate characterization of the melting fraction, so the enhanced model obtained more accurate results [12]. This study further illustrates that the enthalpy-porosity method is of great significance in the field of material phase change. In an analysis of phase change materials, in order to consider the flow of the liquid phase, it is necessary to establish the coupled equations of the heat transfer field and flow field [13]. In fact, research on the characteristics of the pantograph-catenary arc is mostly focused on the field of AC pantograph-catenary arcs, while there are relatively few relevant research results on the DC pantograph arcs as applied to urban rail transit [14]. Therefore, compared with previous work, it is necessary to combine the arc model and the material phase transition model to solve the problem of contact line ablation under the action of the DC pantograph-catenary arc seen in the urban rail system.

Based on the above research, this paper establishes a simulation model suitable for urban rail DC pantograph-catenary arc systems that is based on the theory of magneto-hydrodynamics and that establishes a contact line ablation model based on the enthalpy-porosity method, considering the flow of the molten pool. According to the established mathematical model, the relevant initial conditions are set, and the finite element software COMSOL Multiphysics 5.5 is used to simulate the model. The simulation results are analyzed and the arc temperature characteristics under different arcing times and the heat flux density of the arc that is injected into the contact line surface are explored. The temperature inside the contact line, the distribution of the molten pool and molten pool velocity, and the relationship between arcing time and the contact line molten pool are analyzed. Finally, based on the emission spectrum method, the arc temperature is measured, and the accuracy of the pantograph arc model is verified according to the experimental results.

2. Model Establishment

2.1. Pantograph-Catenary Arc Model

A two-dimensional simplified geometric model of the pantograph-catenary system along the direction of the train is shown in Figure 1. The cross-section of the pantograph slide plate along the direction of the train is a regular rectangle, and the surface in contact with the discharge gap is equivalent to a line segment. The cross-section of the contact line shows an arc shape with two longitudinal grooves, and it is the lower arc-shaped surface that is mainly involved in contact, so the geometric model of the contact surface

is equivalent to a semicircle. The geometric size of the contact line is consistent with the actual size, and the radius of the bottom arc is 7.2 mm. The straight line passing through the center of the upper surface of the pantograph slide plate and the center of the surface below the contact line is defined as the electrode center line, and the abscissa of the points on the line is 0 mm. The center between the two electrode surfaces is defined as the arc center.

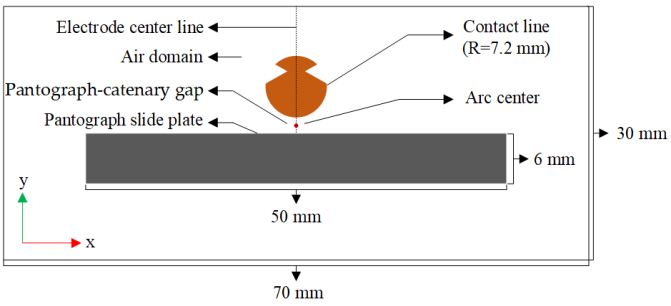

Figure 1. Geometric model of the pantograph-catenary system.

The medium of the pantograph-catenary gap is air, and the change in the physical characteristic parameters of the material in the air domain is provided by the built-in air material function in COMSOL Multiphysics software. The specific physical parameters of the pantograph-catenary system are shown in Table 1.

Table 1. Physical properties of the contact line and pantograph slide plate.

Parameter	Pantograph Slide Plate	Contact Line
Density (kg/m^3)	2.8×10^3	8.7×10^3
Electrical conductivity (S/m)	10^5	5.89×10^7
Thermal conductivity (W/(m·K))	120	400
Specific heat capacity (J/(kg·K))	478	382

The theory of magnetohydrodynamics is based on a combination of traditional fluid mechanics and electromagnetics. It is a discipline that studies the movement of charged fluids in electromagnetic fields [15]. Magnetohydrodynamic theory includes fluid dynamics equations and Maxwell electromagnetic equations.

In order to simplify the model calculation, this paper makes the following assumptions:

1. The solution region of the arc is of incompressible, viscous, Newtonian fluid;
2. The arc plasma is in a local thermal equilibrium state, and does not consider the non-equilibrium state of the electrode region;
3. The flow properties of the flow field in the pantograph-catenary arc are equivalent to laminar flow;
4. The chemical reaction between the arc and the surrounding environment is not considered.

Fluid flow is governed by the physics law of conservation, and the basic conservation equations include mass conservation, momentum conservation, and energy conservation [16].

The mass conservation equation:

$$\frac{\partial \rho}{\partial t} + \rho \nabla \cdot \boldsymbol{u} = 0. \quad (1)$$

ρ is the fluid density; $\boldsymbol{u}$ is the fluid velocity vector.

The momentum conservation equation:

$$\rho\frac{\partial \boldsymbol{u}}{\partial t} + \rho(\boldsymbol{u}\cdot\nabla)\boldsymbol{u} = \nabla\cdot(-p\boldsymbol{I}+\boldsymbol{K}) + \boldsymbol{F} \tag{2}$$

$$\boldsymbol{K} = \mu(\nabla\boldsymbol{u} + (\nabla\boldsymbol{u})^T) \tag{3}$$

$$\boldsymbol{F} = \boldsymbol{J}\times\boldsymbol{B}. \tag{4}$$

p is pressure; $\boldsymbol{I}$ is the unit matrix; μ is dynamic viscosity; $\boldsymbol{F}$ is the momentum source term; $\boldsymbol{J}$ is the current density vector; $\boldsymbol{B}$ is the magnetic induction intensity vector.

The energy conservation equation:

$$\rho C_p\frac{\partial T}{\partial t} + \rho C_p\boldsymbol{u}\cdot\nabla T + \nabla\cdot(-k\nabla T) = Q \tag{5}$$

$$Q = \alpha_p T(\frac{\partial p}{\partial t} + \boldsymbol{u}\cdot\nabla p) + V + \boldsymbol{E}\cdot\boldsymbol{J} - Q_{rad} \tag{6}$$

C_p is constant pressure heat capacity; T is temperature; k is the thermal conductivity; Q is the energy source term; α_p is the thermal expansion coefficient; $\boldsymbol{E}$ is the electric field intensity vector. The first term on the right side of Equation (6) is the work performed by the pressure change; the second term V on the right side of Equation (6) is the viscous dissipation term; the third term on the right side of Equation (6) is Joule heat; the fourth term on the right side of Equation (6) is the volume net radiation loss, which is an inherent physical parameter of air plasma.

Because the arc temperature is very high, the thermal radiation phenomenon is obvious. However, it is very difficult to accurately express thermal radiation. Therefore, in order to simplify the calculation of the arc radiation process, this paper uses the volume net radiation coefficient method to calculate thermal radiation [17]:

$$Q_{rad} = 4\pi\varepsilon_n \tag{7}$$

In the above formula, ε_n is the volume net radiation coefficient related to temperature.

In addition to the above equations, the model also involves electromagnetic field-related equations, as follows.

The potential φ solves the following equations:

$$\nabla\cdot\boldsymbol{J} = 0 \tag{8}$$

$$\boldsymbol{J} = \sigma\boldsymbol{E} \tag{9}$$

$$\boldsymbol{E} = -\nabla\varphi \tag{10}$$

σ is the conductivity.

For the solution of the arc magnetic field, the common methods are the Biot–Savart theorem and the magnetic vector solution equation. Due to the simple calculation and fast calculation speed of the magnetic vector potential solution equation, the magnetic field is calculated by the magnetic vector potential in this paper [18]:

$$\nabla\times\boldsymbol{H} = \boldsymbol{J} \tag{11}$$

$$\boldsymbol{B} = \mu_{\mathrm{r}}\mu_0\boldsymbol{H} \tag{12}$$

$$\boldsymbol{B} = \nabla\times\boldsymbol{A} \tag{13}$$

$\boldsymbol{H}$ is the magnetic field strength; μ_r is the relative permeability, and here, the value is 1; μ_0 is the vacuum permeability; $\boldsymbol{A}$ is the magnetic vector potential.

2.2. Arc Ablation Model of the Contact Line

Since this section only studies the ablation characteristics of the contact line, only a two-dimensional simplified geometric model of the contact line along the direction of the train is drawn up. The lower bottom of the contact line that is directly affected by the arc is set as the heat flux density boundary. All the boundaries of the contact line are supplemented with the boundary conditions for convective heat transfer and surface radiation heat transfer to the environment. The two-dimensional simplified geometric model is shown in Figure 2.

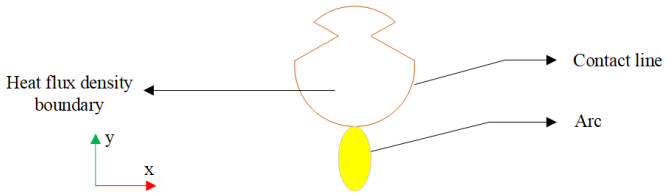

Figure 2. Geometric model of the arc ablation contact line.

The thermal physical property parameters of the contact line are shown in Table 2.

Table 2. Thermal physical property parameters of the contact line.

Parameter	Symbolic Formulation	Value
Melting temperature (K)	T_m	1355
Liquefaction temperature (K)	T_L	1358
Coefficient of thermal expansion (1/K)	β	1.75×10^{-5}
Solid-state specific heat capacity (J/(kg·K))	C_{p0}	382
Melting latent heat (J/kg)	L	3.85×10^{5}
Dynamic viscosity (Pa·s)	μ	0.04
Surface tension coefficient (N/(m·K))	$\partial\gamma/\partial T$	5×10^{-6}

The pantograph-catenary arc can produce a high temperature of tens of thousands of K. The high temperature acts on the contact line, which will melt the surface of the material and form a molten pool, resulting in a solid–liquid phase change. For the solution of the phase transition process, the enthalpy-porosity model is widely used [19]. This method can study the transition of the material from the completely solid phase to the liquid phase, and the transition process is closer to the actual physical process.

In order to simplify the model calculations, this paper makes the following assumptions regarding the contact line ablation model:

1. The liquid region of the contact line is a laminar and incompressible, viscous, Newtonian fluid;
2. When studying the arc ablation characteristics of the material, the evaporation and splash of the molten pool are not considered;
3. The chemical reaction of the electrode material with the arc or with the surrounding environment is not considered;
4. In addition to the specific heat capacity, the thermophysical properties of phase change materials are considered to be independent of temperature, homogeneous, and isotropic.

Control equation:

The material area forming the molten pool satisfies the conservation of mass, momentum, and energy. The governing equation is:

$$\frac{\partial \rho}{\partial t} + \rho \nabla \cdot \boldsymbol{u} = 0 \tag{14}$$

$$\rho\frac{\partial \boldsymbol{u}}{\partial t}+\rho(\boldsymbol{u}\cdot\nabla)\boldsymbol{u}=\nabla\cdot\left[-p\boldsymbol{I}+\mu(\nabla\boldsymbol{u}+(\nabla\boldsymbol{u})^{T})\right]+\boldsymbol{F}_b+\boldsymbol{F}_A \tag{15}$$

$$\rho C_p\frac{\partial T}{\partial t}+\rho C_p\boldsymbol{u}\cdot\nabla T+\nabla\cdot(-k\nabla T)=\beta T(\frac{\partial p}{\partial t}+\boldsymbol{u}\cdot\nabla p)+\tau:\nabla\boldsymbol{u}+Q_{arc} \tag{16}$$

ρ is the contact line density; $\boldsymbol{u}$ is the velocity vector of the molten pool; p is pressure; $\boldsymbol{I}$ is the unit matrix; μ is dynamic viscosity; $\boldsymbol{F}_b$ and $\boldsymbol{F}_A$ are momentum source terms; C_p is the equivalent specific heat capacity of the contact line; T is temperature; k is the thermal conductivity; β is the thermal expansion coefficient of the contact line; τ is the viscous stress tensor, and Q_{arc} is the energy source term, that is, the heat flux density injected by the arc.

In the analysis of the results, the melting of the electrode material under the action of the arc can be analyzed by calculating the liquid phase rate distribution of the contact line material, thereby indicating the degree of arc ablation of the electrode material. The liquid fraction $B(T)$ (also known as the porosity) of liquid components during the phase transition can be expressed as a function of temperature:

$$B(T)=\begin{cases}0, T<(T_m-\Delta T/2)\\ \dfrac{T-T_m+\Delta T/2}{\Delta T}, (T_m-\Delta T/2)\le T<\ (T_m+\Delta T/2)\\ 1, T\ge(T_m+\Delta T/2)\end{cases} \tag{17}$$

T_m is the melting temperature of the contact line; ΔT is the temperature range of the contact line phase transition. The solid phase temperature T_S and liquid phase temperature T_L are, respectively:

$$T_S=T_m-\Delta T/2 \tag{18}$$

$$T_L=T_m+\Delta T/2 \tag{19}$$

For the problem of natural convection in the molten pool, caused by the buoyancy term, a calculation method based on the Boussinesq approximation is used in this paper [20]:

$$\boldsymbol{F}_b=-\boldsymbol{g}\rho\beta(T-T_0) \tag{20}$$

$\boldsymbol{g}$ is the acceleration of gravity; T_0 is the ambient temperature, and the value is 298 K.

When a molten pool is formed on the surface of the material, the solid phase, liquid phase, and mushy area are in the calculation domain. In the solid phase region, there is no flow and no need to solve the momentum equation. In order to extend the solution of the momentum equation to the whole calculation region, the momentum source term is added to the momentum equation with the phase transition process, and its form is obtained according to the Carman–Kozeny model [21]:

$$\boldsymbol{F}_A=S(T)\cdot\boldsymbol{u} \tag{21}$$

$$S(T)=-A_m\frac{(1-B(T))^2}{B(T)^3+b}. \tag{22}$$

A_m is the Carman-Kozeny constant, which is set as a large value, usually between 10^4 and 10^7. In this paper, the value is set at 10^5 during numerical simulation. b is a minimal number, the main function of which is to prevent the denominator from being 0. The smaller the value is, the higher the equivalent accuracy of the corresponding momentum source term. In this paper, the value is 10^{-3}. When $B(T)$ is 1, the material presents a liquid phase and $S(T)$ is 0, and the momentum conservation equation corresponds to the standard Navier–Stokes equation of motion. When $B(T)$ approaches 0, the material gradually takes on a solid phase, and $S(T)$ is a maximum value, thus preventing flow in the solid phase region and limiting the flow speed in the mushy area.

Considering the strong nonlinearity of the phase change process when dealing with the latent heat of melting, this paper uses the equivalent specific heat capacity method to deal with the latent heat of phase change and regards the influence of the latent heat of phase change as the equivalent specific heat capacity, so as to improve the convergence of the calculation. The governing equation is as follows [22]:

$$D(T) = \frac{e^{-\frac{(T-T_m)^2}{(\Delta T/2)^2}}}{\sqrt{\pi(\Delta T/2)^2}} \tag{23}$$

$$C_p(T) = C_{p0} + L \cdot D(T) \tag{24}$$

$D(T)$ is a Gaussian function centered on the transformation temperature T_m; C_{p0} is the solid-state specific heat capacity of the contact line; L is the latent heat of melting of the contact line.

At the bottom boundary of the contact line, the surface of the molten pool is affected by the surface tension and the Marangoni effect, which will affect the flow and temperature distribution of the molten pool and change the growth of the molten pool. Its boundary satisfies the following equation:

$$\left[-p\boldsymbol{I} + \mu(\nabla \boldsymbol{u} + (\nabla \boldsymbol{u})^T)\right]\boldsymbol{n} = \Gamma\gamma\boldsymbol{n} + \frac{\partial\gamma}{\partial T}\nabla \boldsymbol{t}T \tag{25}$$

$\boldsymbol{n}$ is the surface normal vector; Γ is the surface curvature; γ is the surface tension; $\boldsymbol{t}$ is the surface tangent vector; $\partial\gamma/\partial T$ is the surface tension coefficient.

3. Simulation Results and Analysis

3.1. Pantograph-Catenary Arc Temperature Characteristics

When solving the pantograph-catenary arc model, the research time is set to 20 ms, the time step is 0.1 ms, and the pantograph-catenary gap is 4 mm. The relevant boundary conditions and initial values are set as follows. When the heat transfer physical field is set, the initial temperature condition is set to 298 K. In order to reduce the calculation, the left, right, and lower boundaries of the carbon slide plate are set as thermal insulation. The domain thickness is set to 1 m. The air domain is the boundary condition of convective heat transfer. When the current physical field is set, the contact line is set as the cathode of the pantograph-catenary arc, the top boundary of the contact line is set as the boundary current source with a current of 300 A, and the pantograph carbon slide plate is set as the anode of the pantograph-catenary arc. The cathode is used as the emitter to emit the electrons, and the anode is used as the receiving electrode to receive the electrons, so the lower boundary of the carbon slide plate is used as the zero potential boundary condition of the anode. The air domain boundary is the electrical insulation boundary. When the magnetic field is set, the air boundary is set to the magnetic insulation boundary, and the initial value of the magnetic vector potential is 0 Wb/m. For the flow field, the air domain boundary is set as an open boundary, the fluid reference pressure level is set to 1 atm, the airflow rate is set to 10 m/s, and the direction is perpendicular to the cross-section direction of the two-dimensional model.

3.1.1. Pantograph-Catenary Arc Temperature Distribution

Figure 3 shows the simulation results of the pantograph-catenary arc at four moments, with the arc temperature as the characterization parameter.

The whole arc can be observed in the temperature distribution cloud diagrams at different arcing times. It can be seen that:

1. The temperature distribution of the pantograph-catenary arc at different moments along the direction of the train has the characteristics of axisymmetric distribu-

tion and the temperature gradually decreases outward along the center line of the two electrodes.

2. During the initial arcing, the high-temperature region of the arc is small and is mainly concentrated near the surface of the contact line (cathode). With the increase in the arcing time, the high-temperature region of the arc expands outward obviously, and the temperatures near the surface of the two electrodes gradually move closer.
3. The maximum temperature of the arc rises sharply with the increase in the arcing time and the maximum temperature increases by 4440 K within 15 ms.

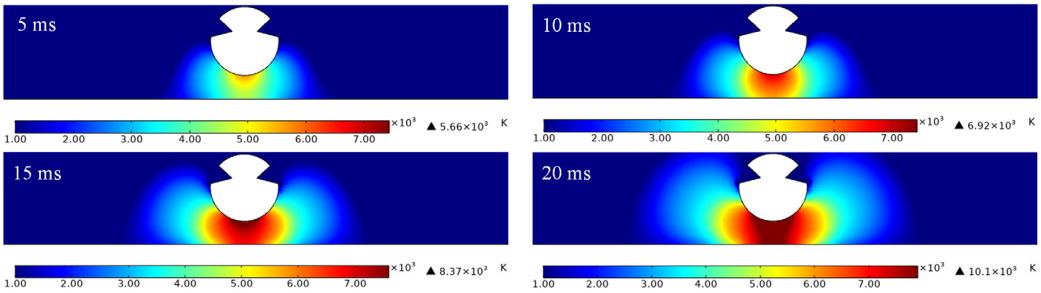

Figure 3. Pantograph-catenary arc temperature distribution cloud.

3.1.2. Distribution of Heat Flux Density on the Contact Line Surface

The heat flux density injected into the contact line is an important parameter for analyzing the ablation of the contact line caused by the pantograph-catenary arc. Therefore, based on the simulation results of the pantograph-catenary arc model, the heat flux density of the arc, injected into the contact line under different arcing times, is extracted, as shown in Figure 4.

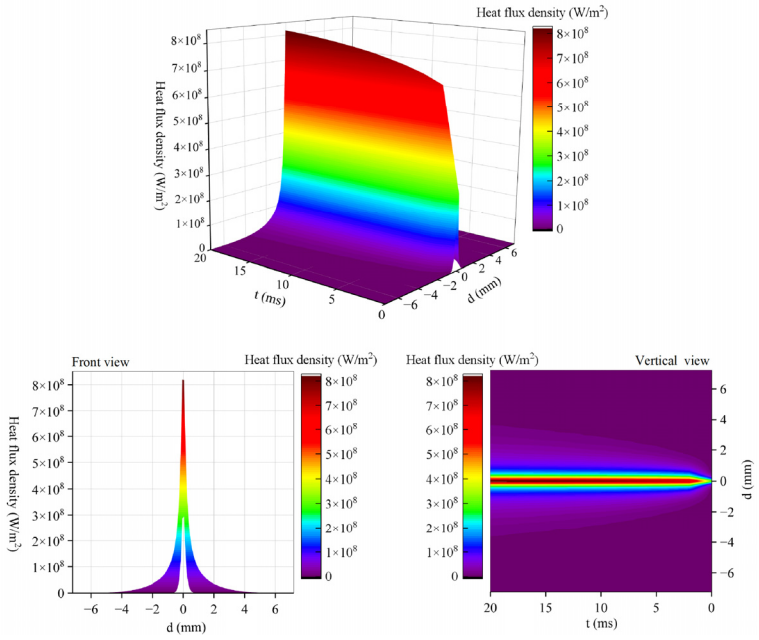

Figure 4. The heat flux density injected into the contact line at different arcing times.

It can be seen from Figure 4 that the main distribution trend of the heat flux density injected into the contact line is that it decreases with the increase in the distance *d* from the central line of the electrode, and its overall distribution shows an approximate Gaussian distribution [23]. In addition, it can be seen from the figure that the heat flux density increases significantly with the increase in arcing time *t*. This is because the increase in arcing time means that the high-temperature region of the arc expands to both sides and

the maximum temperature of the arc increases accordingly. Therefore, the heat flux density injected into the contact line increases with the increase in arcing time.

3.2. Arc Ablation Characteristics of Contact Line

When solving the contact line ablation model, the heat flux density values injected into the contact line, as obtained by solving the pantograph-catenary arc model, are introduced into the contact line ablation model as boundary conditions. The initial values of the temperature and pressure are the same as those in Section 3.1. When the multi-physical field is set, the Marangoni effect is added to the lower bottom of the contact line. The simulation of contact line ablation takes into account the change in material from a solid phase to a liquid phase and the flow of the liquid phase, and the phase transition temperature range of the contact line is small. Therefore, in order to further control the accuracy of the model and the calculation time of the model, the iteration time of each step is set to 0.1 ms, and the total running time is 10 ms.

3.2.1. Analysis of Internal Temperature, the Molten Pool, and the Molten Pool Velocity of the Contact Line

When the contact line material is injected by the arc heat flux density, the temperature rises and transmits to the inside, resulting in melting occurring inside the contact line material. When the melting phenomenon occurs, the liquid phase rate of the material gradually changes from 0 to 1, thus forming a molten pool. The molten pool is affected by driving forces such as thermal buoyancy, which will lead to the flow of the molten pool. In order to analyze the ablation characteristics of the pantograph-catenary arc on the contact line, this section analyzes the simulation results of the contact line temperature, the molten pool, and the molten pool speed when the arcing time is 10 ms, as shown in Figure 5.

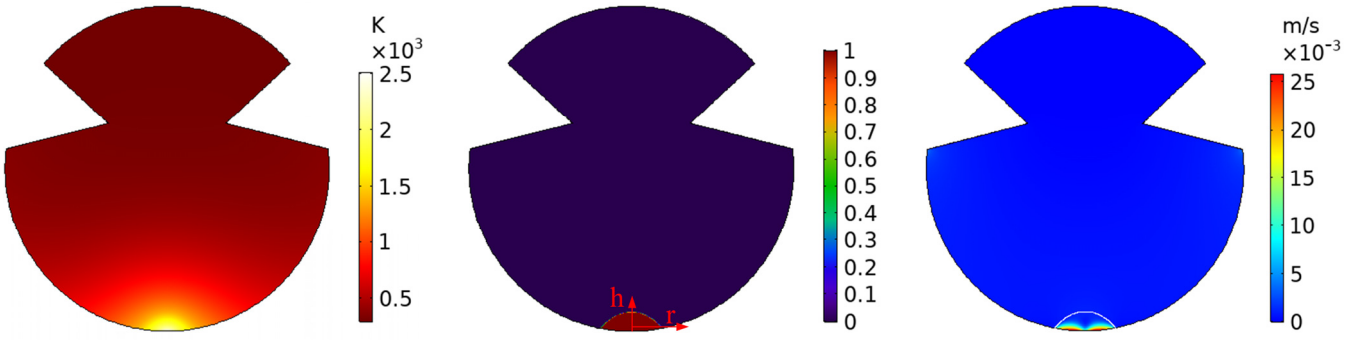

(**a**) (**b**) (**c**)

Figure 5. The distribution of temperature, the molten pool, and molten pool velocity inside the contact line material: (**a**) the distribution of temperature inside the contact line; (**b**) the distribution of the molten pool inside the contact line; (**c**) the distribution of the molten pool velocity inside the contact line.

From Figure 5a, it can be seen that the thermal ablation zone of the contact line material forms an arc shape, and the high-temperature area is also mainly concentrated near the center of the bottom of the contact line. The highest temperature reaches 2510 K, which is more than the melting temperature of the contact line material at 1355 K, and the region above the melting temperature has undergone solid–liquid phase transition.

The distribution of the molten pool of the contact line is shown in Figure 5b. The area with a liquid phase rate of 0 is a solid phase, and the area with a liquid phase rate of 1 is a molten pool with a completely liquid phase, which is the main component of the molten pool. The liquid phase rate between 0 and 1 is a molten pool where the fluid–solid phase coexists, which is distributed at the boundary of the molten pool and is less widely distributed. The overall distribution of the molten pool presents an approximate arc shape,

which also corresponds to the temperature distribution of the contact line in Figure 5a. In order to facilitate an analysis of the distribution of the molten pool, the maximum width of the molten pool from the center line of the electrode to the surface of the contact line is defined as the radius of the molten pool r, and the maximum depth of the molten pool in the vertical direction is defined as the depth of the molten pool h. The radius of the molten pool is 1.259 mm, the depth of the molten pool is 0.788 mm, and the radius of the molten pool is greater than the depth of the molten pool.

Figure 5c shows the distribution of the flow velocity of the contact line molten pool. The temperature contour is set as the velocity result, and the white contour with a temperature of T_S is obtained using the horizontal definition method, that is, the outer contour of the molten pool. It can be seen from Figure 5c that during the formation of the molten pool, its interior is not stationary. Two areas with concentrated velocity distribution from the center of the molten pool to the outside are formed inside the molten pool, and they are approximately symmetrically distributed. The velocity of the molten pool gradually decreases from the bottom of the molten pool to the inside of the molten pool. The maximum velocity of the molten pool reaches 0.0258 m/s, which is distributed on the surface of the contact line. The main reason for this situation is that the surface of the contact line is affected by the Marangoni effect and surface tension. In fact, the flow of the molten pool will accelerate the heat dissipation inside the material, making the heat erosion zone grow.

3.2.2. Variation Law of the Molten Pool at the Contact Line with Arcing Time

In the actual train operation process, the pantograph-catenary arc will last for a certain period of time. The analysis of the temperature characteristics of the pantograph-catenary arc in Section 3.1.1 mentions that as the arcing time increases, the maximum temperature of the arc increases, and the high-temperature area expands. Therefore, it is necessary to study the distribution of the molten pool of the contact line under different arcing times to reflect the arc ablation characteristics of the contact line. Due to the poor convergence of the liquid phase rate distribution in the initial solution of the contact line ablation model, arcing times of 2 ms, 5 ms, 8 ms, and 10 ms are selected as the characteristic values for analysis.

In order to facilitate the observation, this section draws a local view of the contact line containing the molten pool, as shown in Figure 6. According to Figure 6, under the action of the pantograph-catenary arc, the temperature of the contact line reaches the melting point of the material and melts to form a molten pool. From arcing at 2 ms to 10 ms, the overall molten pool of the contact line shows an arc shape with an expanding size.

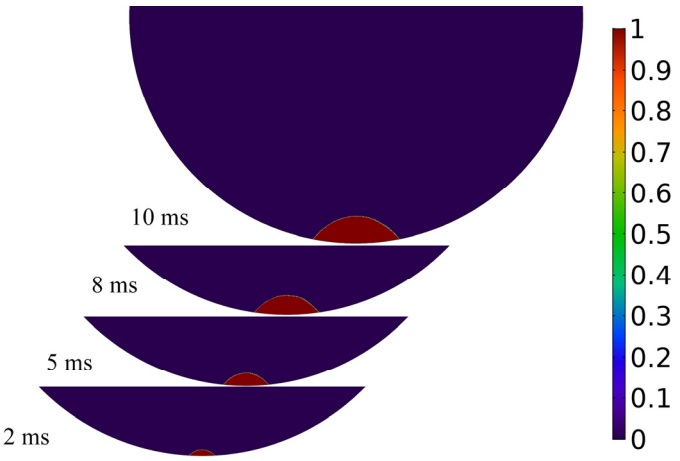

Figure 6. Distribution of the contact line molten pool at different arcing times.

The relationship between the depth h and radius r of the molten pool and the arcing time t is obtained by counting the data in Figure 6, as shown in Figure 7.

It can be seen from Figure 7 that when the duration of the pantograph-catenary arc changes from 2 ms to 10 ms, the radius and depth of the contact line molten pool gradually

increase. The depth of the molten pool changes from 0.184 mm after 2 ms to 0.788 mm after 10 ms. The radius of the molten pool changed from 0.384 mm after 2 ms to 1.259 mm after 10 ms. It can be seen that the radius of the molten pool is always greater than the depth of the molten pool, and the gap between the two *r-h* is gradually increasing with the increase in the arcing time, indicating that the transverse ablation degree of the molten pool is greater than the internal longitudinal ablation degree during the ablation process.

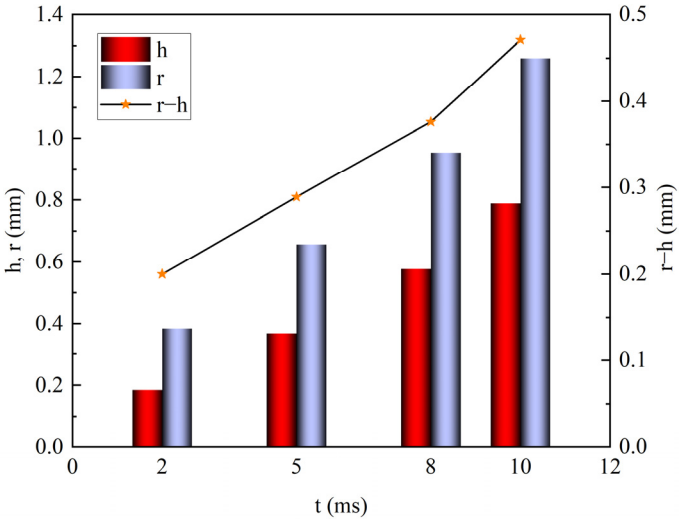

Figure 7. The variation in the depth and radius of the contact line molten pool with the arcing time.

In the COMSOL Multiphysics software, the area where the liquid phase rate is greater than 0 is calculated by the integral method to obtain the molten pool area *S* under different arcing times, as shown in Figure 8.

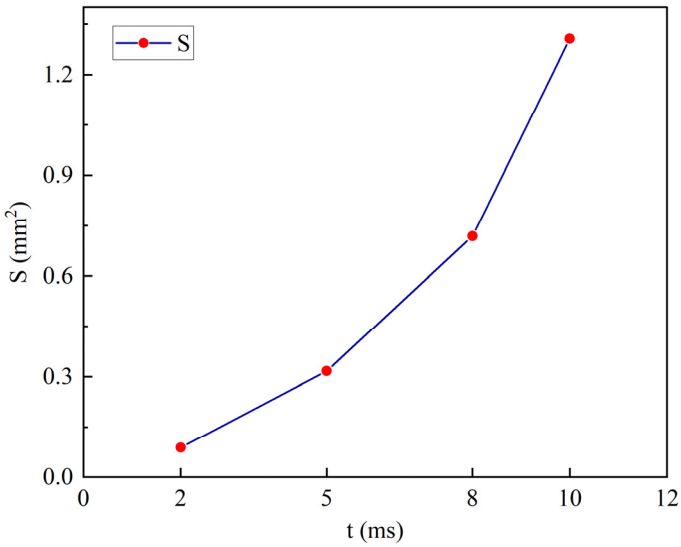

Figure 8. Molten pool area of the contact line after different arcing times.

As can be seen from Figure 8, with the increase in arcing time, the molten pool continues to expand to the surface of the contact line and to corrode the inside of the contact line, resulting in an increasing area of the molten pool on the surface of the contact line from 0.088 mm^2 after 2 ms to 1.307 mm^2 after 10 ms.

In summary, the duration of the pantograph-catenary arc has a significant effect on the ablation of the contact line, and it can be concluded that long-term pantograph-catenary arcing will cause the ablation of the contact line of the pantograph-catenary system to become more serious.

4. Verification of the Simulation Model

The arcing temperature of the arc is extremely high; the central area can reach 10,000 K at its highest temperature, and the arcing time is short. Therefore, the traditional contact measurement method is not suitable for arc temperature measurement. The emission spectroscopy method, which is employed in non-contact diagnosis, has been widely used in arc plasma parameter diagnosis because it does not affect the thermal radiation of the arc plasma, the diagnostic parameters are comprehensive, and the instrument's operation is simple [24]. In this paper, a DC pantograph-catenary arc with 300 A of current is generated by designing a pantograph-catenary arc experiment that is a very close match to the actual working conditions. In the experiment, the rotation of the contact line is adjusted by controlling the motor speed to achieve the required speed, which is set to 10 m/s in this section. The emission spectrum of the pantograph-catenary arc is obtained by the spectrometer. Multiple atomic spectral lines were selected from the spectrum, and the arc temperature of the urban rail pantograph-catenary was calculated using the Boltzmann mapping method, combined with the corresponding parameters from the NIST database. A diagram of the pantograph-catenary arc experimental platform that was made in the laboratory for this study is shown in Figure 9.

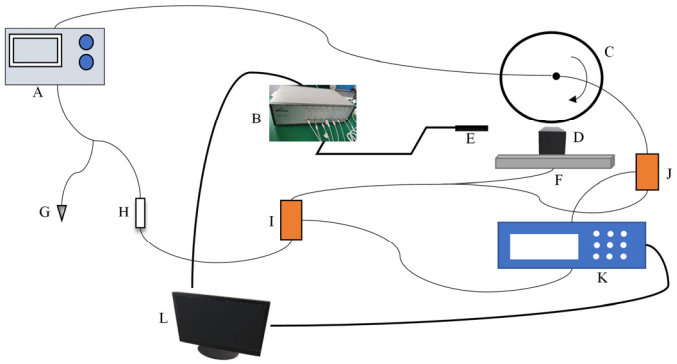

Figure 9. Pantograph-catenary arc experimental platform diagram. A—High voltage power supply, B—Avantes spectrometer, C—contact line, D—pantograph carbon slider, E—fiber optic probe, F—displacement console, G—grounding, H—adjustable resistance, I—current acquisition, J—voltage acquisition, K—data collection, L—calculators.

In the first experiment, the arc temperature at the center point of the two electrodes after different arcing times, under the conditions of a current of 300 A and a pantograph-catenary gap of 4 mm, is obtained. In order to prevent experimental error, three iterations of temperature detection should be carried out on the arc center, following the same test steps. A comparison and analysis of the experimental results for T_2, T_3, and T_4 with the simulation results T_1 are shown in Figure 10.

Comparing the temperature measured by the pantograph-catenary arc test with the temperature obtained by the arc simulation, it is evident that the simulation results and the experimental results also show that the arc temperature increases with the increase in the arcing time, and the temperature errors between the two are small at the same time points. The main reason for the error is that in the simulation, the pantograph-catenary arc model does not consider the influence of the Joule heat generated by the electrode and the chemical reaction between the arc and the surrounding gas on the arc temperature. Therefore, this error is within a reasonable range. After this comparison, it is considered that the pantograph-catenary arc simulation model is basically reliable.

At present, there are no data available for reference on the arc erosion of the contact line, and it is very difficult to measure the molten pool considering the liquid phase flow in real time through experiments alone. In this paper, the heat flux injected into the contact line is derived from the pantograph-catenary arc simulation model. Therefore, the verification of the pantograph-catenary arc model also verifies the reliability of the contact line arc

ablation model, to a certain extent. The analysis of the change in trend of the molten pool and the thermal erosion area of the contact line with different arcing times is consistent with the results reported in the literature [25,26], that is, the depth and radius of the molten pool of the contact line increase with the increase in the arc action time, the thermal erosion area of the contact line shows an arc-shaped expansion and the highest temperature point is close to the surface of the contact line. This further illustrates the rationality of the contact line arc ablation model discussed in this paper.

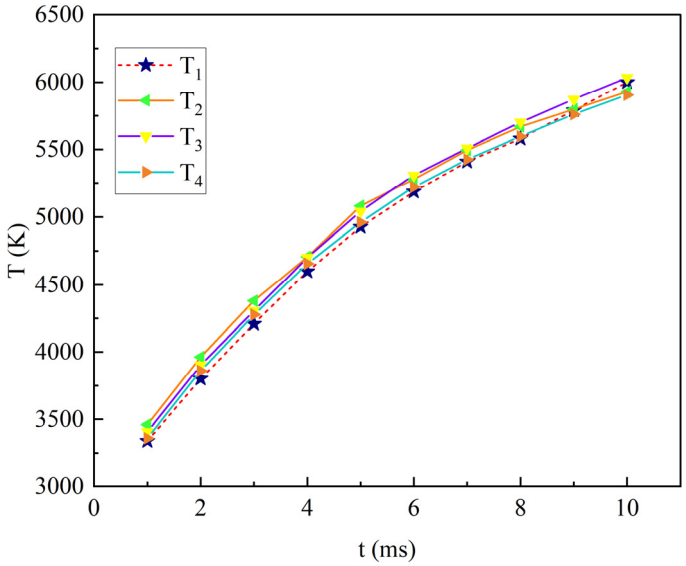

Figure 10. Comparison of the test and simulation results.

5. Conclusions

1. Through an analysis of the simulation results regarding the pantograph-catenary arc temperature, it was found that the high-temperature area of the arc is mainly concentrated near the surface of the contact line (cathode) at the initial stage of arcing. The arc temperature shape at different times is approximately axisymmetric. With an increase in the arcing time, the high-temperature area of the arc also expands outward obviously. The heat flux density of the pantograph-catenary arc on the surface of the contact line has an approximately Gaussian distribution and increases significantly with the increase in arcing time.
2. The high-temperature area of the contact line and the molten pool are distributed in an arc shape, and the surface radius of the molten pool is greater than the depth of the molten pool. The internal flow of the contact line molten pool is basically symmetrically distributed, and the maximum velocity is distributed at the bottom boundary of the contact line. The area, radius, and depth of the molten pool of the contact line are positively correlated with the arcing time. Therefore, with the increase in the arcing time, the arc ablation characteristics of the contact line will be enhanced; the radius of the molten pool is always greater than the depth of the molten pool, which leads to the transverse ablation degree of the molten pool being greater than the longitudinal ablation degree.
3. Based on the emission spectrum method, the temperature of the arc center is obtained by using the laboratory pantograph-catenary arc simulation test system. Comparing the experimental and simulated values, it can be seen that the errors are small, and the variation trend is the same, which indicates that the pantograph-catenary arc model is reliable. Comparing the simulation results of the arc ablation model of the contact line in this paper with the simulation results in the existing literature, it is clear that the distribution of the molten pool and the temperature distribution trend are basically the same, so the effectiveness of the contact line arc ablation model is further verified.

The conclusions of this paper are helpful to further clarify the thermal field distribution of the pantograph-catenary arc and the arc ablation mechanism of the contact line, and the research method herein will be helpful to explore suppression methods of the pantograph-catenary arc and the optimal design of contact lines under the action of the arc, which is of great significance in prolonging the service life of electrode materials.

Author Contributions: Conceptualization, X.Y. and Z.W.; methodology, Z.W.; software, Z.W.; validation, M.S., L.S. and J.Y.; formal analysis, M.S.; investigation, Y.S.; resources, J.Y.; data curation, Z.W.; writing—original draft preparation, X.Y.; writing—review and editing, L.S.; visualization, J.Y.; supervision, X.Y.; project administration, X.Y.; funding acquisition, X.Y. All authors have read and agreed to the published version of the manuscript.

Funding: This work was funded by the Science and Technology Program of Gansu Province (23CXGA0023) and the Science and Technology Research and Development Program of China National Railway Group Corporation Limited (N2022X009).

Data Availability Statement: Data are contained within the article.

Conflicts of Interest: The authors declare no conflicts of interest.

References

1. Li, S.; Ling, Q.; Han, K.; Wen, K. An SD-LV Calculation Model for the Scale of the Urban Rail Transit Network. *Systems* **2024**, *12*, 233. [CrossRef]
2. Li, J.; Cao, Y.; Yang, X.; Hao, J. Simulation of subway tunnel construction process based on fi-nite element analysis. *J. Appl. Sci. Eng.* **2021**, *24*, 783–789. [CrossRef]
3. Tan, M.; Li, H.; Nie, L. Defect Diagnosis of Rigid Catenary System Based on Pantograph Vibration Performance. *Actuators* **2024**, *13*, 162. [CrossRef]
4. Huang, S.; Zhai, Y.; Zhang, M.; Hou, X. Arc detection and recognition in pantograph–catenary system based on convolutional neural network. *Inf. Sci.* **2019**, *501*, 363–376. [CrossRef]
5. Signorino, D.; Giordano, D.; Mariscotti, A.; Gallo, D.; Delle, A.; Balic, F.; Quintana, J.; Donadio, L.; Biancucci, A. Dataset of measured and commented pantograph electric arcs in DC railways. *Data Brief* **2020**, *31*, 105978. [CrossRef]
6. Cho, Y.; Lim, J.; Seo, H.; Bang, S.; Choe, G. A Series Arc Fault Detection Strategy for Single-Phase Boost PFC Rectifiers. *J. Power Electron.* **2015**, *15*, 1664–1672. [CrossRef]
7. Yu, X. Research and Application on Pantograph Arc Detection System of Urban Rail Based on Solar-Blind Region. Ph.D. Thesis, Lanzhou Jiaotong University, Lanzhou, China, 2021. [CrossRef]
8. Zhou, X.; Wang, Y.; Wang, B.; Bai, X.; Fu, J.; Tian, Q. Numerical simulation of effect of overlapping distance on molten pool flow and deposited layer morphology of WAAM. *Trans. Mater. Heat Treat.* **2024**, *45*, 195–204. [CrossRef]
9. Toktaliev, P.; Kazanskii, P.; Moralev, I.; Semenyov, P.; Martynenko, S. Study of the influence of current pulse parameters on kinematic and energy characteristics of a plasma actuator based on a moving electric arc. *Int. J. Heat Mass Transf.* **2023**, *201*, 123661. [CrossRef]
10. Sunar, Ö.; Fletcher, D. Experimental Investigation on the Arc Damage and Fatigue Crack Initiation Risk of Copper-Silver Contact Wires. *IEEE Trans. Power Deliv.* **2022**, *38*, 777–784. [CrossRef]
11. Wu, Y. Study on Pantograph-Catenary Arc and the Arc Erosion Characteristics of Pantograph and Catenary Materials. Master's Thesis, Southwest Jiaotong University, Chengdu, China, 2019. [CrossRef]
12. Sabine, M.; Robert, D. Influence of Natural Convection and Volume Change on Numerical Simulation of Phase Change Materials for Latent Heat Storage. *Energies* **2022**, *15*, 2746. [CrossRef]
13. Vogel, J. Influence of Natural Convection on Melting of Phase Change Materials. Ph.D. Thesis, University of Stuttgart, Stuttgart, Germany, 2019. [CrossRef]
14. Wang, J. Research on the Key Characteristics of DC Pantograph Arc. Master's Thesis, Liaoning Technical University, Fuxin, China, 2021. [CrossRef]
15. Song, M.; Yu, X.; Wang, Z.; Su, Y.; Yang, J. Research on multiphysical field simulation of pantograph arc in urban rail transit based on COMSOL. *J. Northwest Norm. Univ. (Nat. Sci.)* **2024**, *60*, 46–51. [CrossRef]
16. Zhu, G.; Wu, G.; Han, W.; Gao, G.; Liu, X. Simulation and Analysis of Pantograph-catenary Arc Steady-state Characteristics during Static Lifting and Lowering of High-speed Railway Pantograph. *J. China Railw. Soc.* **2016**, *38*, 42–47. [CrossRef]
17. Xu, Z.; Gao, G.; Wei, W.; Yang, Z.; Xie, W.; Dong, K.; Ma, Y.; Yang, Y.; Wu, G. Characteristics of pantograph-catenary arc under low air pressure and strong airflow. *High Volt.* **2022**, *7*, 369–381. [CrossRef]
18. Li, S.; Li, Z.; Yang, X.; Kang, Y.; Dong, H. Simulation Study on Arc Temperature Field Characteristics of Oil-immersed On-load Tap-changer. *J. Electr. Eng.* **2023**, *18*, 135–144.
19. Han, T.; Mao, Y.; Fang, J.; Yan, H.; Wei, J.; Dong, S. Numerical simulation study of heat transfer characteristics on solar tube-and-shell phase change heat storage unit. *Acta Energiae Solaris Sin.* **2023**, *44*, 525–532. [CrossRef]

20. Groulx, D.; Biwole, H. Solar PV Passive Temperature Control Using Phase Change Materials. *Int. Heat Transf. Conf.* **2014**, *15*, 8187–8201. [CrossRef]
21. Voller, V.; Prakash, C. A fixed grid numerical modelling methodology for convection-diffusion mushy region phase-change problems. *Int. J. Heat Mass Transf.* **1987**, *30*, 1709–1719. [CrossRef]
22. Bachmann, M.; Avilov, V.; Gumenyuk, A.; Rethmeier, M. About the influence of a steady magnetic field on weld pool dynamics in partial penetration high power laser beam welding of thick aluminium parts. *Int. J. Heat Mass Transf.* **2013**, *60*, 309–321. [CrossRef]
23. Hao, J.; Gao, G.; Xu, P.; Wei, W.; Hu, Y.; Wu, G. Model of Coupled Pantograph-catenary Arc and Electrodes Considering Electrodes Melting. *High Volt. Eng.* **2018**, *44*, 1668–1676. [CrossRef]
24. Yuan, Y.; Tian, L.; Guo, C.; Zhao, Q. Spectral diagnosis of an arc jet actuator. *Chin. Opt.* **2023**, *16*, 296–304. [CrossRef]
25. Wu, Y.; Yang, Z.; Gao, G.; Wei, W.; Li, C.; Wu, G. Thermal Ablation Process of Electrical Contact Materials Under Arc Effect. *High Volt. Eng.* **2019**, *45*, 2276–2283. [CrossRef]
26. Hao, J. Study on the Dynamics of Pantograph-Catenary Arc and the Erosion Effect of Pantograph-Catenary Arc on the Pantograph and Catenary. Master's Thesis, Southwest Jiaotong University, Chengdu, China, 2017.